PCCP

Molecular-Scale Origins of Solution Nanostructure and Excess Thermodynamic Properties in a Water/Amphiphile Mixture

Journal:	*Physical Chemistry Chemical Physics*
Manuscript ID	CP-ART-01-2021-000082.R1
Article Type:	Paper
Date Submitted by the Author:	25-Feb-2021
Complete List of Authors:	Servis, Michael; Argonne National Laboratory Piechowicz, Marek; Argonne National Laboratory Skanthakumar, Suntharalimgam; U.S. Department of Energy, Argonne National Laboratory Soderholm, L.; Argonne National Laboratory, Chemical Sciences and Engineering Division

Molecular-Scale Origins of Solution Nanostructure and Excess Thermodynamic Properties in a Water/Amphiphile Mixture

[1] Michael J. Servis,* Marek Piechowicz, S. Skanthakumar, and L. Soderholm

Chemical Sciences and Engineering Division, Argonne National Laboratory, Argonne, IL 60439

E-mail: mservis@anl.gov

Abstract

Quantifying the molecular and nanoscale origins of nonideality in excess thermodynamic properties are essential to understanding cosolvent mixtures, yet they remain challenging to determine. Here, we consider a binary mixture of water and an amphiphile, *N,N,N',N'*-tetramethylmalonamide (TMMA), which is characterized by strong hydrogen bonding between the two components and no hydrogen bonding between amphiphiles. Using molecular dynamics simulation, validated with excess volume measurements and X-ray scattering, we identify three distinct solution regimes across the composition range of the binary mixture and find that the transition between two of these regimes, marked by the water percolation threshold, is closely correlated with minima in the excess volume and excess enthalpy. Structural analysis of the simulations reveals an interplay between local interactions and solution nanostructure, determined by the relative strength of the water-water and water-amphiphile hydrogen bonding interactions. By comparison to other amphiphiles, such as linear alcohols, the relative strength of like and unlike interactions between water and amphiphile affects the relationship between thermodynamics and structural regimes. This provides insight into how molecular forces of mutual solvation interact across length scales and how they manifest in excess thermodynamic properties.

Introduction

Nonideal binary mixtures of miscible solvents are macroscopically homogeneous, yet often feature microheterogeneity on the nanoscale.[1–7] The heterogeneity of a given mixture depends on the molecular structures and intermolecular interactions of its constituent cosolvents.[8,9] On the bulk scale these interactions determine the sign and magnitude of important excess thermodynamic properties, including the excess volume as well as the excess enthalpy and entropy of mixing. These properties determine the utility of mixtures for various applications, while also providing insight into the intermolecular interactions that define the mixture. While excess thermodynamic properties are experimentally accessible, attribution to solution structuring and the specific intermolecular interactions driving that structure is essential to designing effective mixtures for a targeted application.[10–15] Connecting these length scales, spanning from the molecular to macroscopic, is a fundamental objective of research on liquid mixtures.[16]

In this study, we consider aqueous/amphiphile mixtures. Structuring in these solutions is driven by hydrogen bonding: between water molecules, between water and the amphiphile, and in some cases, between the amphiphile molecules. The competitive effects of hydrogen bonding, hydrophobic solvation and interconnectivity of water and amphiphile hydrogen bonding networks lead to rich solution behaviors, which often depend strongly on the molecular structure of the amphiphile.[8] Significant progress has been made in understanding these mixtures.[14,17–23] Phenomena associated with water/alcohol systems,[2,8–10,12,15,24–36] including anomalous negative excess entropy, have been the subject of study for decades.[10,27,37] More broadly, the hydrogen bonding networks of water/alcohol mixtures are proposed to be connected to thermodynamic anomalies.[38,39] Recent advances in understanding[40–43] highlight the intricate complexity of these simple systems and demonstrate the power of new experimental and computational approaches to probe their molecular structure.

Here, we connect the nanoscale behavior of a water/amphiphile mixture to its thermodynamic mixing properties. We consider a mixture of water and an amidic amphiphile,

N,N,N',N'-tetramethylmalonamide (TMMA), that, when immobilized onto a polymer resin,[44,45] or functionalized with alkyl tails,[46,47] is commonly utilized as a metal ion complexant in chemical separations processes. As a binary liquid mixture, this system is characterized by a scalar compositional variable; here we use the TMMA mole fraction, χ_{TMMA}. The water/TMMA binary mixture is made distinct from water/alcohol mixtures by the absence of hydrogen bonding between amphiphile molecules and the strong hydrogen bonding cross-interaction between the water and amphiphile. The resulting combination of intermolecular interactions provides rich nanostructuring across the range of compositions for this binary system and provides a complement to commonly studied water/alcohol solutions. Using this binary mixture, we investigate the competition between intermolecular interactions driving mutual solvation by employing molecular dynamics (MD) simulations, validated by direct comparison with experimentally determined excess volumes of mixing and molecular correlations obtained from X-ray scattering.[48,49] Using this multimodal approach we assess the impact of hydrogen bonding on solution nanostructure and macroscopic thermodynamic properties, finding that intermolecular interactions compete with nanoscopic organization to determine the extrema in excess thermdodynamic properties.

Methodology

Experiments

TMMA was purchased from TCI chemicals in 97% assay measured via GC and used as received. Water content in neat TMMA was measured in triplicate using the Karl-Fischer apparatus with injected sample mass measured to 0.1 mg accuracy. Densities of TMMA/water solutions were measured using an Anton Paar densitometer via direct injection into an oscillating U-tube. Comparison of densities across the TMMA/mole fraction range at 25° and 30° is shown in Figure S1. Experimental mole fractions of water/TMMA mixtures were measured volumetrically and corrected for the atmospheric water content in neat TMMA.

X-ray scattering experiments were conducted in transmission geometry using beamline 11-ID-B at the Advanced Photon Source, Argonne National Laboratory, operating at an incident photon energy of 86.7 keV. A series of TMMA/water samples, with TMMA mole fractions ranging from 0 to 1, were made by measuring mass with 0.1 mg accuracy and loaded in 1.5mm Kapton capillaries for data acquisition. Scattered intensities were measured using a Perkin Elmer XRD1621 amorphous silicon flat-panel detector mounted in a static position at two different sample-to-detector distances, providing a total q range of 0.26 to 35 Å^{-1}.

Simulation

Simulation compositions are provided in Table 1. The smallest non-zero water content system ($\chi_{\text{TMMA}} = 0.967$) corresponds to the amount of atmospheric water measured in neat TMMA. The GROMACS 2016.2 software package[50] was used to conduct molecular dynamics simulations. The GAFF2[51] force field was used for TMMA and TIP4P-ew[52] model for water. Partial atomic charges for TMMA were generated with Primadorac[53] using the AM1-BCC method[54] and are reported in the SI with the GROMACS input topology file for TMMA, in addition to the TMMA Lennard-Jones parameters (applied with Lorentz-Berthelot mixing rules). Random initial configurations were generated with Packmol[55] and energy minimized with a steepest decent algorithm. Simulations were conducted with a leap-frog Verlet integrator[56] using a 2 fs time step. Hydrogen-containing bonds were constrained using the LINCS algorithm.[57] Long-range electrostatic interactions were computed with Particle-Mesh Ewald summation[58] with a 1.5 nm cutoff for short-range electrostatics and Lennard-Jones interactions.

Temperature and pressure were set to 300 K and 1 bar. The velocity rescale thermostat[59] with a 0.2 ps coupling time and Berendsen barostat[59] with a 2 ps coupling time were used during NPT, while the Nosé-Hoover thermostat[60] was used with a 0.2 ps coupling during NVT. The system was equilibrated for 5 ns in NPT, with reported volumes averaged over the last 1 ns, followed by 10 ns of NVT equilibration and 50 ns of NVT production, which was

sampling at 100 ps intervals for analysis. An additional 100 ns of production was conducted for the lower water concentration systems ($\chi_{\mathrm{TMMA}} \geq 0.423$) to improve statistical accuracy of the water oxygen-oxygen RDFs and water cluster size distributions. Data from these extended simulations for those properties are plotted in Figure S3 and S4, respectively. X-ray scattering profiles from simulations were calculated using the approach described by Walter et al.[61] In addition, due to the high q-range, we account for the q-dependent incoherent scattering contribution to the simulation scattering pattern.[49]

Table 1: The simulation compositions and periodic box sizes.

TMMA mole fraction, χ_{TMMA}	TMMA num.	Water num.	Simulation box length (nm)
0.000	0	7218	5.94
0.007	47	6857	5.95
0.031	187	5775	5.96
0.079	374	4331	5.97
0.162	560	2887	5.99
0.232	654	2166	6.01
0.341	747	1444	6.03
0.371	766	1299	6.03
0.423	794	1083	6.05
0.538	841	722	6.05
0.711	887	361	6.07
0.807	906	217	6.08
0.967	930	29	6.09
1.000	934	0	6.09

Hydrogen bonding and clustering

Hydrogen bonds were defined between two water molecules or between water and the carbonyl oxygen of TMMA by O...H distances of up to 0.25 nm and O-H...O angles of at least 145°. Water clusters are defined from resulting the water-water hydrogen bonding network as connected components of the graph which is defined by water molecules (nodes) and hydrogen bonds between those molecules (edges) using the ChemNetworks software package.[62] TMMA clusters are defined with edges constructed between TMMA molecules based on the

distance between "central carbon" atoms (carbon bridging amide groups, referred to as CC) using a distance cutoff of 0.62 nm, which is taken from the first minimum of the CC-CC RDFs (plotted below). Cluster size distributions are the ensemble average number of each cluster size observed in the simulation. Figure S3 shows that determination of the percolation threshold from cluster size distributions for water does not depend strongly on hydrogen bond definition. Water oxygen-oxygen RDFs are given in Figure S4.

Excess thermodynamic properties

Derived excess properties are denoted with superscript E, while measured quantities are denoted with brackets. The excess enthalpy of mixing, ΔH^E is defined as

$$\Delta H^E = \langle U \rangle_m - \sum_i \chi_i \langle U \rangle_i + pV^E, \tag{1}$$

where p is the pressure and $\langle U \rangle_m$ is the average internal energy of the mixture and $\langle U \rangle_i$ is the average internal energy for the pure phase for component i (in this case TMMA or water), with χ_i being the mole fraction of that component.[63] The excess volume, V^E is defined similarly, with

$$V^E = \langle V \rangle_m - \sum_i \chi_i \langle V \rangle_i. \tag{2}$$

For the experimental excess volume measurements, the density, rather than volume, is measured, and the excess volume is therefore defined as[64]

$$V^E = \langle V \rangle_m - \sum_i \frac{\chi_i M_i}{\rho_i}, \tag{3}$$

where M_i and ρ_i are the molar mass and density, respectively, of the pure phases for component i. The excess water-water hydrogen bonding per water, n^E_{HB}, is obtained from simulation with

$$n^E_{\mathrm{HB}} = \langle n_{\mathrm{HB}} \rangle_m - \sum_i \chi_i \langle n_{\mathrm{HB}} \rangle_i, \tag{4}$$

noting that there is no water hydrogen bonding in the pure TMMA phase.

Results

Results from the MD simulations reveal three distinct regimes for the TMMA/water mixture: water-rich, TMMA-rich, and an intermediate regime with bipercolating networks of water and TMMA. These three regimes are illustrated in Figure 1 with snapshots showing the structure of the water-rich and TMMA-rich systems as well as the two boundary compositions of the bipercolating regime. In the following we describe these regimes, and the transitions between them, in order of ascending χ_{TMMA}.

The water-rich regime exists at low χ_{TMMA}. Upon the addition of small amounts of TMMA to pure water, the carbonyl oxygens accept strong hydrogen bonds from water. This is demonstrated by the negative excess water-water hydrogen bonding and growth of water-TMMA hydrogen bonding, shown in the left and center panels of Figure 2. The sharp decrease in excess enthalpy (Figure 3) in this regime, despite the net decrease in total water hydrogen bonding, is attributed to the enthalpic strength of the water-TMMA hydrogen bond. Further, the decrease in excess volume, also shown in Figure 3, is attributed to the improved packing of mixtures of small and large particles, with a TMMA molecule occupying nearly 10× the volume of a water in their respective pure phases. (We note that the good agreement between simulation and experiment for the excess volume—a stringent test of force field compatibility—lends confidence to the simulation structures and, by virtue of the simulation reproducing the χ_{TMMA} value of the excess volume minimum, the simulation-assigned concentrations of the structural transitions.) In addition to hydrogen bonding at the carbonyl sites, water molecules maintain their hydrogen bonding network around the nonpolar regions of the TMMA molecules, illustrated in the right panel of Figure 2. This is consistent with aqueous solvation of hydrophobic solutes.[65,66] While TMMA forms, on average, nearly three hydrogen bonds with water at low χ_{TMMA}, TMMA molecules still

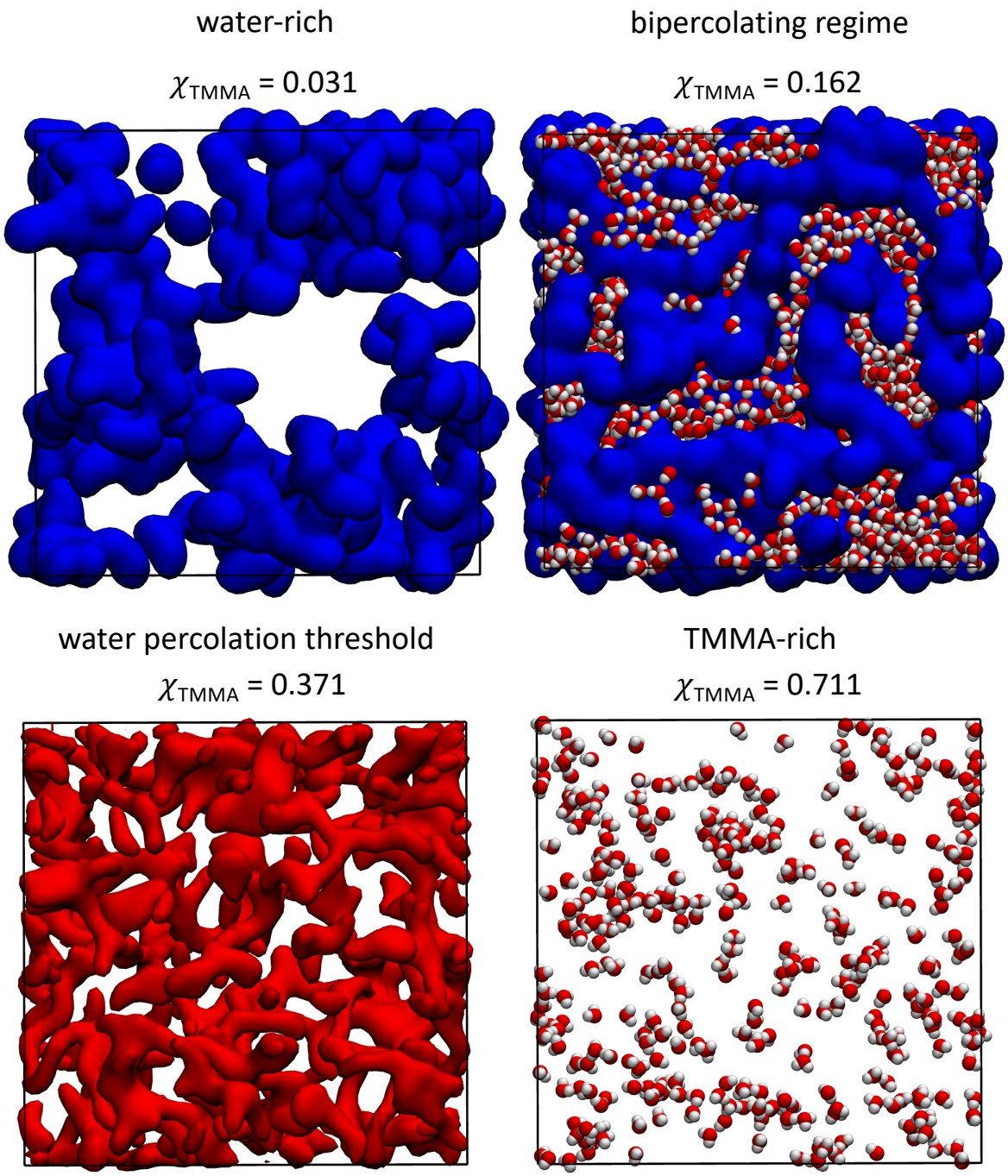

Figure 1: Snapshots are shown for four compositions: $\chi_{\mathrm{TMMA}} = 0.031$ (water-rich regime, upper left), $\chi_{\mathrm{TMMA}} = 0.162$ (water-rich boundary of bipercolating regime, upper right), $\chi_{\mathrm{TMMA}} = 0.371$ (TMMA-rich boundary of bipercolating regime, lower left), $\chi_{\mathrm{TMMA}} = 0.711$ (TMMA-rich regime, lower right). Surface-type depictions of water are drawn in red and molecular-type depictions with oxygen drawn in red and hydrogen in white. Surface-type depictions of TMMA are drawn in blue.

cluster in solution, as shown in Figure 1, creating loosely structured hydrophobic assemblies.

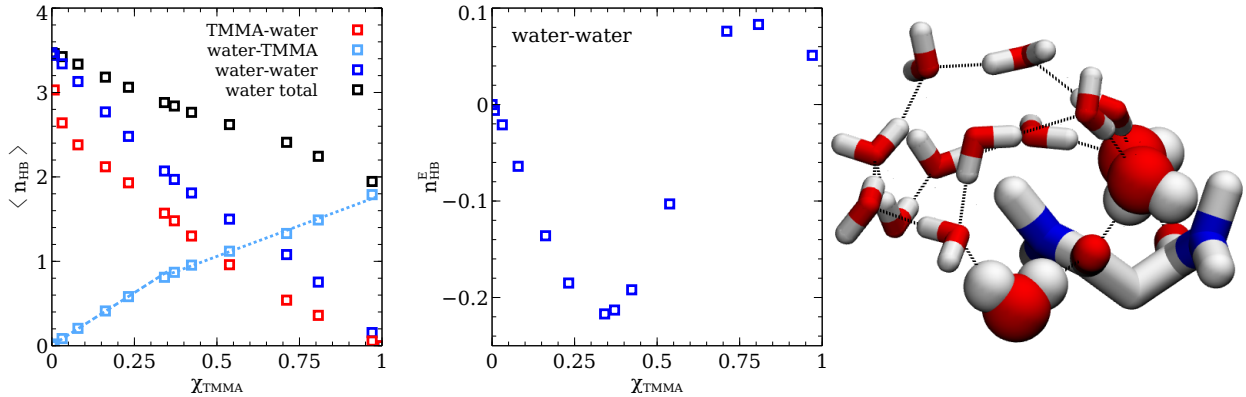

Figure 2: The average number of hydrogen bonds are plotted for each simulation in the left panel. Numbers for molecule pairs are normalized by the first molecule listed. Linear fits of the change in water-TMMA hydrogen bonds are shown as dashed line from $\chi_{\mathrm{TMMA}} = 0.007$ to 0.371 and from 0.423 to 0.967. The excess water-water hydrogen bonds are plotted in the center panel. On the right, water hydrogen bonding with the carbonyl oxygen of TMMA (drawn as spherical) and water hydrogen bonding around the hydrophobic region of TMMA are illustrated with a snapshot. Oxygen atoms are drawn in red, hydrogen in white and nitrogen in blue.

To identify the transition between the water-rich regime (characterized by TMMA clustering) and the bipercolating regime (characterized by a spanning TMMA network interpersed with the spanning water network), we consider carbon-carbon radial distribution functions (RDFs), $g(r)$, computed from the MD simulations. Figure 4 shows validation of simulation structures by comparison of calculated[61] X-ray scattering patterns computed for all atoms to experimental X-ray scattering intensities as a function of scattering vector, $I(q)$, across the composition range. Details about the experimental scattering data and their Fourier transforms are provided in the SI. While the X-ray scattering data contain contributions from all atom pairs, specific atom pairs are accessible from the RDFs of the MD simulations. Figure 5 shows the CC-CC and C-C RDFs, respectively, where CC is the central carbon that bridges amide groups and C-C counts atom pairs for all carbon atoms sites. TMMA clustering is evident from the long-range order observed in these RDFs. Long-range carbon-carbon correlations ($r \geq 0.7$ nm) decrease with increasing TMMA concentration up to $\chi_{\mathrm{TMMA}} = 0.162$, as seen from Figure 5. Meanwhile, $g(r)$ for higher concentrations quickly reach bulk density

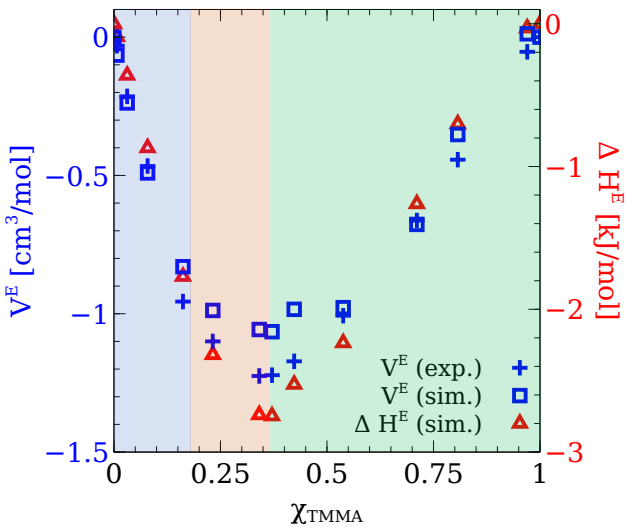

Figure 3: In the left panel, the percent excess volumes (left axis) are plotted for the simulations (squares) and experiments (crosses) with blue symbols. Excess enthalpies of mixing (right axis) for the simulation data are drawn with red squares. In the right panel, the the excess enthalpy for each composition is plotted against the percent excess volumes, with arrows indicating the clockwise path of increasing χ_{TMMA}. Regions are color-coded: blue is water-rich, orange is bipercolating and green is TMMA-rich.

with subtle oscillations between 0.7 and 1.0 nm. Therefore, the TMMA-TMMA correlations show that the transition from hydrophobic clustering to a stable, system-spanning network occurs between $\chi_{\mathrm{TMMA}} = 0.162$ and 0.232.

This interpretation is corroborated by cluster analysis of the TMMA molecules, plotted in Figure 6. At high χ_{TMMA}, the TMMA cluster distribution is dominated by the system-spanning cluster, manifested as a sharp peak at large cluster size, with the exact size determined by the number of molecules in the periodic simulation box. As χ_{TMMA} decreases, the spanning network decreases in size as the number of TMMA molecules in the simulations decreases. This behavior is accompanied by the in-growth of populations of smaller, discrete clusters. The $\chi_{\mathrm{TMMA}} = 0.162$ and 0.232 cluster size distributions nearly follow a power law, with slope consistent with the Fisher exponent for percolation in three dimensions, $\tau = 2.19$.[67] The $\chi_{\mathrm{TMMA}} = 0.162$ cluster distribution appears to be just below the percolation threshold, and the $\chi_{\mathrm{TMMA}} = 0.232$ system just after, with the system-spanning cluster growing in at large cluster sizes for $\chi_{\mathrm{TMMA}} > 0.232$. Therefore, we expect the percolation

threshold to fall between those two compositions. While the choice of cutoff for TMMA connectivity is arbitrary, particularly compared to the natural definition of hydrogen bonding connectivity for water clustering, the TMMA cluster distribution percolation threshold is consistent with the interpretation of the carbon-carbon and CC-CC RDFs, lending confidence to the choice of cutoff and physical meaning of the cluster analysis.

Within the bipercolating regime, the two components are mutually dispersed, forming separate, but spanning, percolating networks, resulting in nanoscopic segregation of the two solvents. This region of the binary mixture is characterized by significant surface area between the two mutually miscible solvent networks, maximizing the favorable TMMA-water hydrogen bonds responsible for the complete miscibility of the mixture. In this regime, the addition of TMMA continues to increase TMMA-water hydrogen bonding, as shown in Figure 2, which further lowers the excess enthalpy of the mixture. However, TMMA cannot be added to the TMMA domains indefinitely, as, eventually, it will disrupt the ability of the water network to percolate.

The end of the bipercolating regime and transition to the TMMA-rich mixtures is demarcated by the water percolation threshold, with water no longer percolating in the TMMA-rich regime. This transition is apparent from the water cluster distributions given in Figure 7. At $\chi_{\mathrm{TMMA}} = 0.371$, the percolation threshold is reached, with the cluster size distribution following a power law with the expected slope, as seen for TMMA at the TMMA percolation threshold. (Figure S3 shows that the χ_{TMMA} value of the water percolation transition does not strongly depend on the hydrogen bond definition. Water oxygen-oxygen RDFs are given in Figure S4.) The filamentous structure of the water hydrogen bonded network at the percolation threshold is illustrated in Figure 1. The water percolation transition is approximately coincident with the minima in the excess enthalpy and volume (Figure 3), as well as the minimum in the excess water-water hydrogen bonding (Figure 2).

Finally, in the TMMA-rich region, water forms only small, discrete clusters as water-TMMA hydrogen bonding continues to grow with increasing χ_{TMMA} at the expense of water-

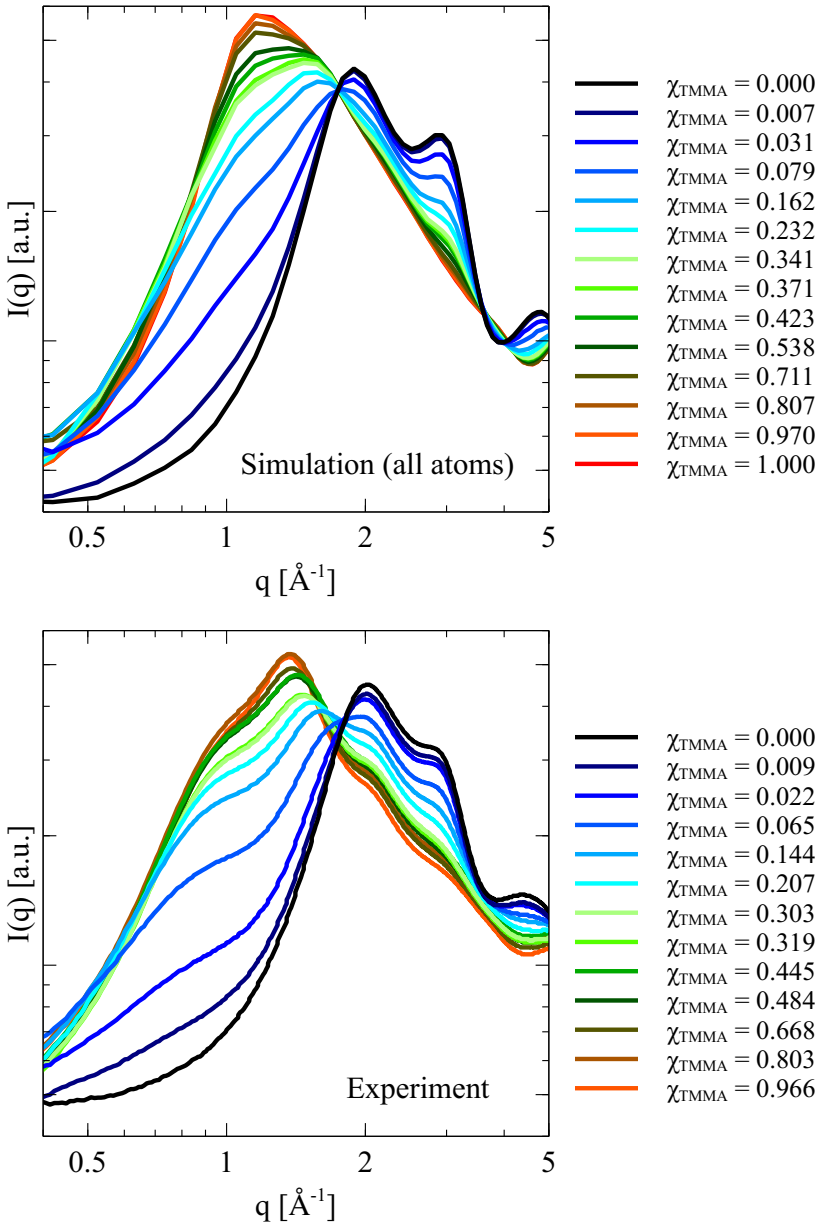

Figure 4: Simulation calculated X-ray scattering intensities for all atoms (top) are compared with experimental data (bottom).

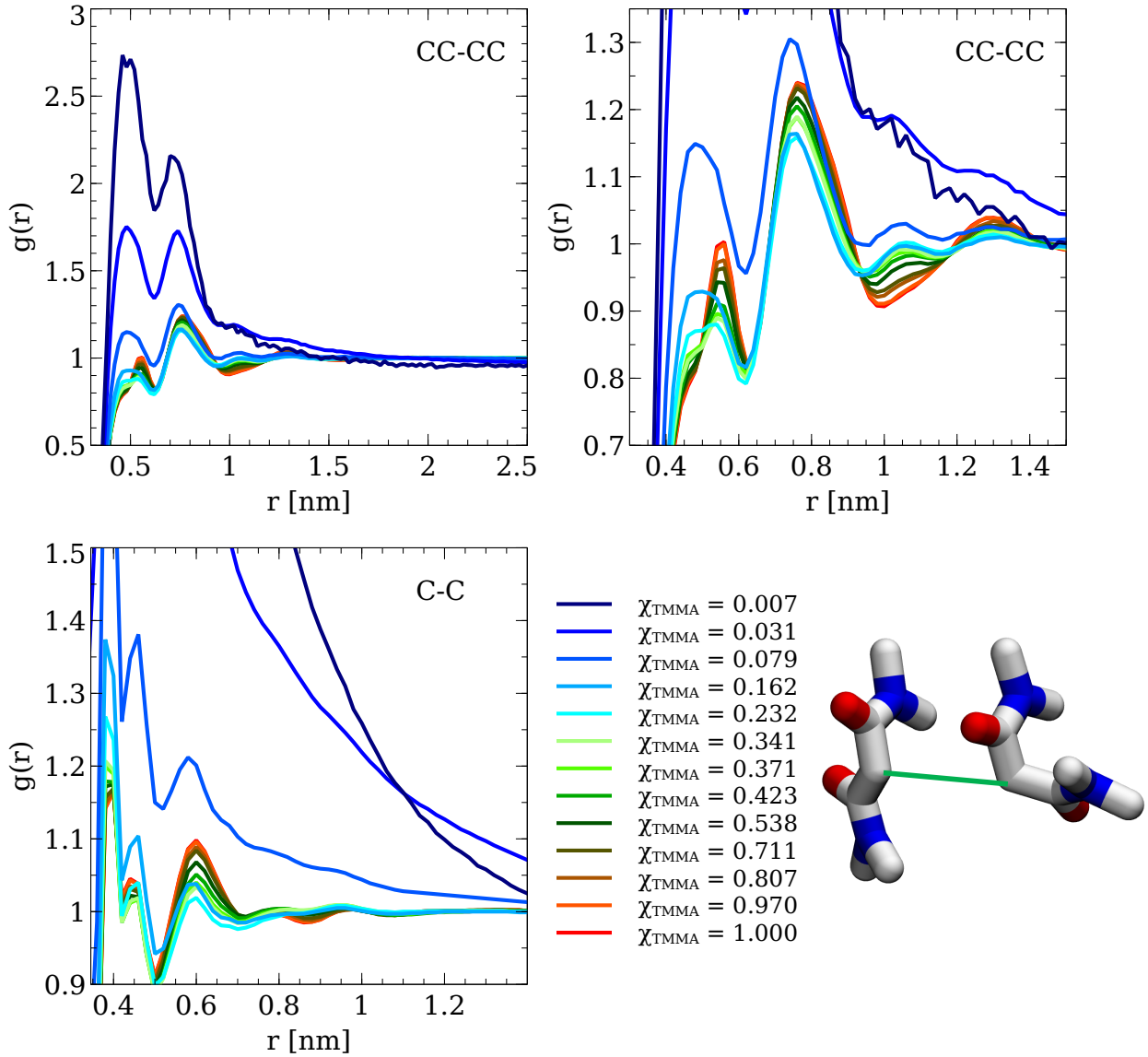

Figure 5: The CC-CC RDFs (as illustrated in lower right snapshot) are shown in the upper left panel and upper right panels. The RDFs between all carbon atom sites are shown in the lower left panel.

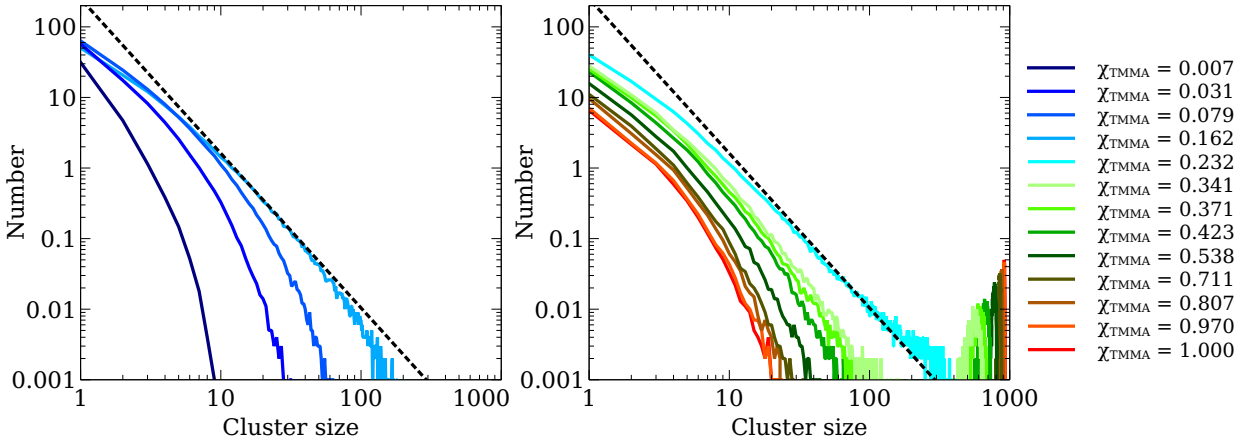

Figure 6: The TMMA cluster size distributions are plotted for each simulation, with lower TMMA concentrations (below the percolation threshold) in the left panel and higher concentrations (above the percolation threshold) in the right. The theoretical distribution for percolation in three dimensions is overlayed with a dotted black line.

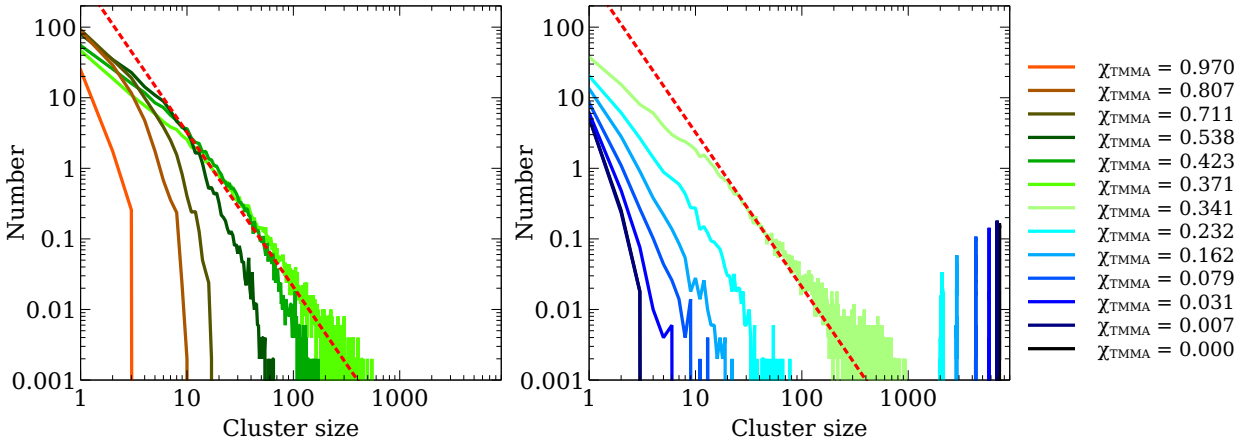

Figure 7: The water cluster size distributions are plotted for each simulation, with lower water concentrations (up to and including the percolation threshold) in the left panel and higher concentrations (beyond the percolation threshold) in the right. The theoretical distribution for percolation in three dimensions is overlayed with a dotted red line.

water hydrogen bonding. However, differential addition of TMMA creates fewer additional water-TMMA hydrogen bonds per water (Figure 2). Instead, excess water-water hydrogen bonding begins to increase, until it finally becomes positive, with a maximum near the $\chi_{\mathrm{TMMA}} = 0.803$ composition. This indicates that under these conditions water preferentially self-associates, as seen in Figure 1, forming discrete water clusters lacking a characteristic size (the water cluster sizes are, within statistical accuracy, approximately exponentially distributed below the percolation threshold, at $\chi_{\mathrm{TMMA}} \geq 0.423$). Finally, approaching pure TMMA, the excess water-water hydrogen bonding returns to zero, with nearly all water molecules donating two hydrogen bonds to TMMA.

Lastly, we comment on the conformation of TMMA and its relationship to solution conditions. The TMMA molecule is flexible and interconverts between *gauche* and *trans* conformations, corresponding to, respectively, approximately aligned and antiparallel C=O bond vectors, as illustrated in Figure 8. (The O=C−N−Me groups are always planar.) We assign *gauche* and *trans* based on the angle between the C=O vectors of the 5-member pseudo dihedral (O=C−C−C=O). This distribution, given in Figure 8, shows a natural cutoff of 120 degrees to distinguish the conformations. The interconversion between conformations is quick, and the relative populations equilibrate during the first half nanosecond of the 5 ns of NPT equilibration, as shown in Figure 8, after which the average fraction of each conformer is constant during the production trajectory. The ratio of conformers depends on the solution conditions, with the higher dipole *gauche* conformation more common under more polar solution conditions, i.e., at lower TMMA mole fractions. Figure 8 shows the fraction of *gauche* conformers for each composition, with the average number of water-TMMA hydrogen bonds per TMMA to highlight how TMMA conformation tracks with solvation by water, particularly in the water-rich regime, before approaching a *gauche* fraction of about 0.1 in the limit of no water and therefore no hydrogen bonding.

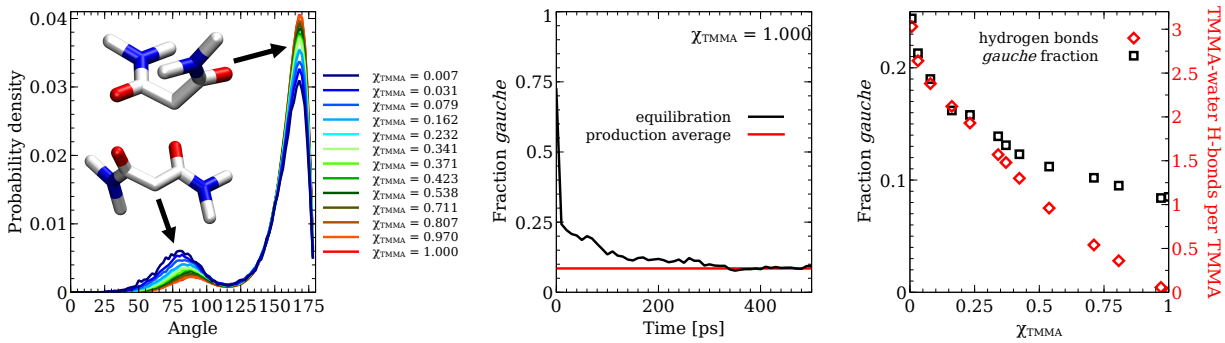

Figure 8: In the left panel, the distribution of inter-C=O angles for each system is plotted, with the populations corresponding to *trans* (top inset) and *gauche* (bottom inset) illustrated with snapshots. In the center panel, the fraction of *gauche* TMMA molecules is plotted versus time during the first 500 ps of NPT equilibration (black) and compared to the NVT production trajectory ensemble average (red) for the $\chi_{\mathrm{TMMA}} = 1.000$ system. In the right panel, the fraction of TMMA in the *gauche* conformation are plotted as a function of composition (black squares, left axis) and compared to the average number of TMMA-water hydrogen bonds per TMMA molecule (red diamonds, right axis).

Discussion

The properties of the binary mixture are dominated by the water-TMMA hydrogen bond. This strong cross-interaction between the two components keeps the mixture miscible at all volume fractions and is responsible for the bipercolating networks at intermediate compositions. By contrast, while alcohols with larger aliphatic groups (such as *n*-butanol) are reported to disrupt water hydrogen bonding, thereby limiting the miscibility of that binary mixture,[15] the water-TMMA interaction is sufficiently strong compared to water-alcohol hydrogen bonding that, despite the large size of TMMA, they remain completely miscible. We attribute the location of the excess enthalpy minimum to the balance between maximizing water-TMMA hydrogen bonding while maintaining the water-water hydrogen bond network. The minimum occurs at the composition with the maximum amount of TMMA (and therefore water-TMMA hydrogen bonding, as it increases monotonically with χ_{TMMA}, see Figure 2) before the water network is successfully disrupted and no longer percolates (see Figure 7). This disruption of the water network results from dominance of the water-TMMA hydrogen bonding over that of water-water as well as the reduction in total water available to form

the water hydrogen bonded network as χ_{TMMA} increases. There is a clear transition in slope of water-TMMA hydrogen bonds versus χ_{TMMA} upon reaching the TMMA-rich regime, as illustrated in Figure 2. There, the approximately linear relationship between χ_{TMMA} and the number of water-TMMA hydrogen bonds per water changes slope from 2.50 to 1.46. The significant change in hydrogen bonding behavior illustrates the loss of interconnectivity between the two components once the spanning water network is disrupted. The coincidence with the minimum in mixing enthalpy illustrates the competition between maximizing the number of favorable local interactions (increasing χ_{TMMA} to increase water-TMMA hydrogen bonding) while maintaining the nanostructure that supports high interconnectivity (not increasing χ_{TMMA} to preserve the bipercolating networks).

The minimum in excess volume is also attributed to a competition across length scales. The minimum excess volume (i.e., the most efficient packing) occurs under nearly the same conditions as the minimum in excess enthalpy: at the highest possible χ_{TMMA} while maintaining the bipercolating networks. Overall, the negative excess volume results from the poor packing of TMMA and the more efficient packing afforded by mixing large (TMMA) and small (water) particles. This contribution is not expected to occur with solution components of equal size. The minimum in excess volume occurs at the boundary of the bipercolating regime and TMMA-rich regimes, just before TMMA breaks up the spanning water network. From the χ_{TMMA} of the minimum excess volume, decreasing χ_{TMMA} corresponds to more water-rich bipercolating solutions, which increases the excess volume by reducing the total amount of poorly-packing TMMA that is efficiently solvated by water. Meanwhile, increase in χ_{TMMA} from the minimum disrupts the water network, preventing the water from adequately solvating the TMMA, instead forming the poorly-packing TMMA-rich morphology. For the excess volume as well as excess enthalpy, the persistence of the mesoscopic spanning water network competes with local effects (hydrogen bonding for enthalpy, packing for volume) to determine the minima in the thermodynamic properties.

The competition of forces described above provides a complementary comparison to other

binary mixtures. For example, with longer-chain malonamides, such as the oil-soluble extractants used in liquid-liquid extraction, the observed solution nanoscale structuring in the absence of water (or any other solutes that enable strong, directional interactions) is dominated by dipole-dipole association of the amphiphile in nonpolar solvents.[68] By contrast, the water/TMMA mixture features relatively weak inter-amphiphile interactions but a strong, dominant interaction between solvents. This behavior also contrasts with commonly studied water/alcohol mixtures. For water/methanol mixtures—which are not dominated by a strong cross-interaction between water and amphiphile[69]—the excess enthalpy minimum is observed near $\chi_{\mathrm{MeOH}} = 0.3$ and the excess volume minimum near $\chi_{\mathrm{MeOH}} = 0.5$.[36,70–73] These mole fractions are qualitatively consistent with percolation transitions reported in the literature for water/methanol mixtures. Dougan et al. found that defining methanol clusters by a methyl-methyl cut off distance of 0.57 nm results in a percolated methanol network at $\chi_{\mathrm{MeOH}} \geq 0.27$.[38] (Ghoufi et al.[29] note that ethanol does not form a spanning hydrogen bonded network even in the pure alcohol limit; the network defined by methyl-methyl contacts would certainly percolate under those conditions.) Further, Dougan et al. found that water percolates for $\chi_{\mathrm{MeOH}} \leq 0.54$. Therefore, the excess volume and enthalpy minima are possibly associated with different structural transitions (water percolation versus amphiphile percolation) for the water/methanol mixture, rather than the same transition as observed for the water/TMMA mixture. However, the χ_{MeOH} resolution with which those percolation thresholds were determined is not high. As a result, the excess thermodynamic property minima may be less closely co-located with the percolation transitions than we observe for the water/TMMA mixture. Regardless, the coincidence of the mixing enthalpy and mixing volume minima found for TMMA/water is not observed for water/alcohol mixtures. This indicates a difference in the competition between local and nanoscopic forces, attributed to the stronger cross interaction in the TMMA-water case driving the enthalpy minimum to the composition which maximizes TMMA-water hydrogen bonds (and minimizes the excess water-water hydrogen bonds) while still maintaining the spanning water network. Overall,

this comparison to water mixtures with short chain alcohols highlights how tuning like and unlike interactions in binary water/amphiphile mixtures impacts the fundamental relationships between local interactions, nanoscale solution structure and thermodynamics.

Significant debate surrounds the origins of the anomalous positive excess entropy found in various binary aqueous mixtures. The "iceberg" hypothesis—where water structure is enhanced by the second component, creating additional tetrahedrally ordered (ice-like) water—has recently come under significant scrutiny.[40–43] Recent studies propose instead that nanoscale segregation is responsible for the increased entropy of various alcohol/water mixtures. Our findings are consistent with this latter explanation. The excess water-water hydrogen bonding at low χ_{TMMA} is negative upon addition of TMMA, demonstrating that TMMA does not increase water structure. Further, the solution structures reported here are highly heterogeneous, consistent with the excluded volumes which are proposed as the origin of entropic loss in other mixtures.[30,74,75]

The intermolecular interactions of the water/TMMA mixture create asymmetry in solution behavior across the composition range. The observed TMMA clustering in the low χ_{TMMA} is consistent with hydrophobic assembly,[65] where nonpolar regions of the amphiphilic TMMA associate, minimizing the amount of nonpolar moities exposed to the water solvent. However, instead of a crossover to two distinct macroscopic phases at a sufficiently high concentration of TMMA, the strong cross interaction between TMMA and water keeps the two solvents mutually soluble. The resulting bipercolating regime maximize water-TMMA hydrogen bonding while maintaining nanoscale solvent partitioning. Meanwhile, water clustering at high χ_{TMMA} is not analogous to TMMA clustering at low χ_{TMMA}: water is more well dispersed in the TMMA-rich mixtures. The populations of water-water and water-TMMA hydrogen bonding, and their derivatives with respect to the compositional variable, change with solution regimes, presumably in response to the different solution nanostructures. This suggests solution morphology could play a role in hydrogen bonding-controlled solvation phenomena inherent to solvent mixtures, such as cononsolvency.[24,76,77]

Conclusion

In conclusion, we combine simulation and experiment to probe the role of hydrogen bonding on nanoscale structuring in a binary solvent mixture chosen to accentuate the dominant intersolvent interaction. Using this approach enabled the identification of the molecular drivers for the solution structuring and their link to thermodynamic properties. A close correspondence of X-ray scattering patterns calculated from MD simulations and those determined experimentally provides confidence in the molecular-scale structural results while the agreement between simulation and experimental excess volumes shows the robustness of these results on the macroscopic scale. The cross-scale validation allowed the determination of three morphologically distinct composition regimes: a water-rich, TMMA-rich, and an intermediate regime with bipercolating, simultaneously spanning TMMA and water networks, all driven by the evolving role of TMMA-water hydrogen bonding across the concentration range. The impact of that hydrogen bonding interaction suggests how tuning like and unlike interactions in water/amphiphile mixtures the competition of solvation forces across length scales. These results can serve as one end-point for studies of more complex systems, where competing intrasolvent hydrogen bonding of the amphiphile or the addition of solutes complicates the molecular-scale assignment of bulk phase thermodynamic properties. A robust understanding of the origins of solution nonidealities will facilitate the design of solvent mixtures targeted to specific thermodynamic properties, including nanostructured morphologies optimized for selectivity in chemical separations. From a fundamental perspective, this study will help unravel the molecular origins of thermodynamics and nanostructure and, more broadly, provide insight into hierarchical structure in complex solution phases such as those encountered in biological systems or processes applied to complex material synthesis.

Acknowledgments

This work was supported by U.S. Department of Energy (DOE), Office of Science, Office of Basic Energy Sciences, Chemical Sciences, Geosciences, and Biosciences Division under Contract DE-AC02-06CH11357 to UChicago Argonne, LLC, Operator of Argonne National Laboratory ("Argonne"). Utilized resources include the high-energy scattering beamline 11-ID-B at the Advanced Photon Source, a U.S. DOE Office of Science User Facility operated for the DOE Office of Science by Argonne National Laboratory under the same contract number. We thank Olaf Borkiewicz for their assistance in collecting X-ray scattering data. We gratefully acknowledge the computing resources provided on Bebop, a high-performance computing cluster operated by the Laboratory Computing Resource Center at Argonne National Laboratory.

References

(1) Marcus, Y.; Migron, Y. Polarity, hydrogen bonding, and structure of mixtures of water and cyanomethane. *The Journal of Physical Chemistry* **1991**, *95*, 400–406.

(2) Dixit, S.; Crain, J.; Poon, W.; Finney, J. L.; Soper, A. K. Molecular segregation observed in a concentrated alcohol–water solution. *Nature* **2002**, *416*, 829–832.

(3) Perera, A.; Kežić, B. Fluctuations and micro-heterogeneity in mixtures of complex liquids. *Faraday Discussions* **2013**, *167*, 145–158.

(4) Kežić, B.; Perera, A. Aqueous tert-butanol mixtures: a model for molecular-emulsions. *The Journal of Chemical Physics* **2012**, *137*, 014501.

(5) Kežić, B.; Perera, A. Revisiting aqueous-acetone mixtures through the concept of molecular emulsions. *The Journal of Chemical Physics* **2012**, *137*, 134502.

(6) Kežić, B.; Mazighi, R.; Perera, A. A model for molecular emulsions: Water and "weak

water" mixtures. *Physica A: Statistical Mechanics and its Applications* **2013**, *392*, 567–582.

(7) Perera, A. Molecular emulsions: from charge order to domain order. *Physical Chemistry Chemical Physics* **2017**, *19*, 28275–28285.

(8) Lam, R. K.; Smith, J. W.; Saykally, R. J. Communication: Hydrogen bonding interactions in water-alcohol mixtures from X-ray absorption spectroscopy. *The Journal of Chemical Physics* **2016**, *144*, 191103.

(9) Furlan, A. P.; Lomba, E.; Barbosa, M. Temperature of maximum density and excess properties of short-chain alcohol aqueous solutions: A simplified model simulation study. *The Journal of Chemical Physics* **2017**, *146*, 144503.

(10) Koga, Y.; Nishikawa, K.; Westh, P. "Icebergs" or no "icebergs" in aqueous alcohols?: composition-dependent mixing schemes. *The Journal of Physical Chemistry A* **2004**, *108*, 3873–3877.

(11) Li, R.; D'Agostino, C.; McGregor, J.; Mantle, M. D.; Zeitler, J. A.; Gladden, L. F. Mesoscopic structuring and dynamics of alcohol/water solutions probed by terahertz time-domain spectroscopy and pulsed field gradient nuclear magnetic resonance. *The Journal of Physical Chemistry B* **2014**, *118*, 10156–10166.

(12) Muñoz-Muñoz, Y. M.; Guevara-Carrion, G.; Vrabec, J. Molecular insight into the liquid propan-2-ol+ water mixture. *The Journal of Physical Chemistry B* **2018**, *122*, 8718–8729.

(13) Oh, K.-I.; You, X.; Flanagan, J. C.; Baiz, C. R. Liquid–Liquid Phase Separation Produces Fast H-Bond Dynamics in DMSO–Water Mixtures. *The Journal of Physical Chemistry Letters* **2020**, *11*, 1903–1908.

(14) Zhang, X.; Zhang, L.; Jin, T.; Zhang, Q.; Zhuang, W. Cosolvent effect on the dynamics of water in aqueous binary mixtures. *Molecular Physics* **2018**, *116*, 1014–1025.

(15) Choi, S.; Parameswaran, S.; Choi, J.-H. Understanding alcohol aggregates and the water hydrogen bond network towards miscibility in alcohol solutions: graph theoretical analysis. *Physical Chemistry Chemical Physics* **2020**, *22*, 17181–17195.

(16) Oh, K.-I.; Baiz, C. R. Molecular heterogeneity in aqueous cosolvent systems. *The Journal of Chemical Physics* **2020**, *152*, 190901.

(17) Mountain, R. D. Molecular dynamics study of water- acetonitrile mixtures. *The Journal of Physical Chemistry A* **1999**, *103*, 10744–10748.

(18) Bakó, I.; Megyes, T.; Pálinkás, G. Structural investigation of water–acetonitrile mixtures: An ab initio, molecular dynamics and X-ray diffraction study. *Chemical Physics* **2005**, *316*, 235–244.

(19) Takamuku, T.; Tabata, M.; Yamaguchi, A.; Nishimoto, J.; Kumamoto, M.; Wakita, H.; Yamaguchi, T. Liquid structure of acetonitrile- water mixtures by X-ray diffraction and infrared spectroscopy. *The Journal of Physical Chemistry B* **1998**, *102*, 8880–8888.

(20) Jamroz, D.; Stangret, J.; Lindgren, J. An infrared spectroscopic study of the preferential solvation in water-acetonitrile mixtures. *Journal of the American Chemical Society* **1993**, *115*, 6165–6168.

(21) Stokes, R. Excess partial molar enthalpies for (acetonitrile+ water) from 278 to 318 K. *The Journal of Chemical Thermodynamics* **1987**, *19*, 977–983.

(22) Essafri, I.; Ghoufi, A. Microstructure of nonideal methanol binary liquid mixtures. *Physical Review E* **2019**, *99*, 062607.

(23) Guan, X.; Huang, Z.; Lu, H.; Sun, D. Microheterogeneity and CO2 Switchability of N,

N-Dimethylcyclohexylamine–Water Binary Mixtures. *The Journal of Physical Chemistry B* **2019**, *123*, 3096–3102.

(24) Zuo, T.; Ma, C.; Jiao, G.; Han, Z.; Xiao, S.; Liang, H.; Hong, L.; Bowron, D.; Soper, A.; Han, C. C., et al. Water/Cosolvent Attraction Induced Phase Separation: A Molecular Picture of Cononsolvency. *Macromolecules* **2019**, *52*, 457–464.

(25) Mallamace, D.; Chen, S.-H.; Corsaro, C.; Fazio, E.; Mallamace, F.; Stanley, H. E. Hydrophilic and hydrophobic competition in water-methanol solutions. *SCIENCE CHINA Physics, Mechanics & Astronomy* **2019**, *62*, 107003.

(26) Mallamace, F.; Corsaro, C.; Mallamace, D.; Vasi, C.; Vasi, S.; Stanley, H. E. Dynamical properties of water-methanol solutions. *The Journal of Chemical Physics* **2016**, *144*, 064506.

(27) Noskov, S. Y.; Lamoureux, G.; Roux, B. Molecular dynamics study of hydration in ethanol- water mixtures using a polarizable force field. *The Journal of Physical Chemistry B* **2005**, *109*, 6705–6713.

(28) Mochizuki, K.; Koga, K. Cononsolvency behavior of hydrophobes in water+ methanol mixtures. *Physical Chemistry Chemical Physics* **2016**, *18*, 16188–16195.

(29) Ghoufi, A.; Artzner, F.; Malfreyt, P. Physical properties and hydrogen-bonding network of water–ethanol mixtures from molecular dynamics simulations. *The Journal of Physical Chemistry B* **2016**, *120*, 793–802.

(30) Guo, J.-H.; Luo, Y.; Augustsson, A.; Kashtanov, S.; Rubensson, J.-E.; Shuh, D. K.; Ågren, H.; Nordgren, J. Molecular structure of alcohol-water mixtures. *Physical Review Letters* **2003**, *91*, 157401.

(31) Pothoczki, S.; Pusztai, L.; Bakó, I. Variations of the Hydrogen Bonding and Hydrogen-

Bonded Network in Ethanol–Water Mixtures on Cooling. *The Journal of Physical Chemistry B* **2018**, *122*, 6790–6800.

(32) Dougan, L.; Crain, J.; Finney, J. L.; Soper, A. K. Molecular self-assembly in a model amphiphile system. *Physical Chemistry Chemical Physics* **2010**, *12*, 10221–10229.

(33) Bakó, I.; Megyes, T.; Bálint, S.; Grósz, T.; Chihaia, V. Water–methanol mixtures: topology of hydrogen bonded network. *Physical Chemistry Chemical Physics* **2008**, *10*, 5004–5011.

(34) Bakó, I.; Bencsura, Á.; Hermannson, K.; Bálint, S.; Grósz, T.; Chihaia, V.; Oláh, J. Hydrogen bond network topology in liquid water and methanol: a graph theory approach. *Physical Chemistry Chemical Physics* **2013**, *15*, 15163–15171.

(35) Galicia-Andrés, E.; Pusztai, L.; Temleitner, L.; Pizio, O. Microscopic structure of methanol–water mixtures: Synchrotron X-ray diffraction experiments and molecular dynamics simulations over the entire composition range. *Journal of Molecular Liquids* **2015**, *209*, 586–595.

(36) Galicia-Andrés, E.; Dominguez, H.; Pusztai, L.; Pizio, O. Composition dependence of thermodynamic, dynamic and dielectric properties of water–methanol model mixtures. Molecular dynamics simulation results with the OPLS-AA model for methanol. *Journal of Molecular Liquids* **2015**, *212*, 70–78.

(37) Frank, H. S.; Evans, M. W. Free volume and entropy in condensed systems III. Entropy in binary liquid mixtures; partial molal entropy in dilute solutions; structure and thermodynamics in aqueous electrolytes. *The Journal of Chemical Physics* **1945**, *13*, 507–532.

(38) Dougan, L.; Bates, S.; Hargreaves, R.; Fox, J.; Crain, J.; Finney, J.; Reat, V.; Soper, A. Methanol-water solutions: A bi-percolating liquid mixture. *The Journal of chemical physics* **2004**, *121*, 6456–6462.

(39) Dougan, L.; Hargreaves, R.; Bates, S.; Finney, J.; Reat, V.; Soper, A.; Crain, J. Segregation in aqueous methanol enhanced by cooling and compression. *The Journal of Chemical Physics* **2005**, *122*, 174514.

(40) Galamba, N. Water's structure around hydrophobic solutes and the iceberg model. *The Journal of Physical Chemistry B* **2013**, *117*, 2153–2159.

(41) Graziano, G. Comment on "Water's structure around hydrophobic solutes and the iceberg model". *The Journal of Physical Chemistry B* **2014**, *118*, 2598–2599.

(42) Ben-Naim, A. Myths and verities in protein folding theories: From Frank and Evans iceberg-conjecture to explanation of the hydrophobic effect. *The Journal of Chemical Physics* **2013**, *139*, 10B626_1.

(43) Pascal, T. A.; Goddard III, W. A. Hydrophobic segregation, phase transitions and the anomalous thermodynamics of water/methanol mixtures. *The Journal of Physical Chemistry B* **2012**, *116*, 13905–13912.

(44) Yang, Y.; Alexandratos, S. D. Mechanism of ionic recognition by polymer-supported reagents: immobilized tetramethylmalonamide and the complexation of lanthanide ions. *Inorganic Chemistry* **2010**, *49*, 1008–1016.

(45) Shimada, A.; Sulakova, J.; Yang, Y.; Alexandratos, S.; Nash, K. L. Studies on the Uptake and Column Chromatographic Separation of Eu, Th, U, and Am by Tetramethylmalonamide Resin. *Solvent Extraction and Ion Exchange* **2014**, *32*, 27–43.

(46) Bonnaffé-Moity, M.; Ouadi, A.; Mazan, V.; Miroshnichenko, S.; Ternova, D.; Georg, S.; Sypula, M.; Gaillard, C.; Billard, I. Comparison of uranyl extraction mechanisms in an ionic liquid by use of malonamide or malonamide-functionalized ionic liquid. *Dalton Transactions* **2012**, *41*, 7526–7536.

(47) Spjuth, L.; Liljenzin, J.; Skålberg, M.; Hudson, M.; Chan, G.; Drew, M.; Feaviour, M.; Iveson, P.; Madic, C. Extraction of actinides and lanthanides from nitric acid solution by malonamides. *Radiochimica Acta* **1997**, *78*, 39–46.

(48) Soderholm, L.; Skanthakumar, S.; Neuefeind, J. Determination of actinide speciation in solution using high-energy X-ray scattering. *Analytical and Bioanalytical Chemistry* **2005**, *383*, 48–55.

(49) Egami, T.; Billinge, S. *Underneath the Bragg Peaks: Structural Analysis of Complex Materials*; Pergamon Materials Series; Elsevier Science, 2003.

(50) Abraham, M.; Murtol, T.; Schulz, R.; Pall, S.; Smith, J.; Hess, B.; Lindhal, E. GROMACS: High performance molecular simulations through multi-level parallelism from laptops to supercomputers. *SoftwareX* **2015**, *1-2*, 19–25.

(51) Wang, J.; Wolf, R.; Caldwell, J.; Kollman, P.; Case, D. Development and testing of a general amber force field. *Journal of Computational Chemistry* **2004**, *25*, 1157–1174.

(52) Horn, H. W.; Swope, W. C.; Pitera, J. W.; Madura, J. D.; Dick, T. J.; Hura, G. L.; Head-Gordon, T. Development of an improved four-site water model for biomolecular simulations: TIP4P-Ew. *The Journal of Chemical Physics* **2004**, *120*, 9665–9678.

(53) Procacci, P. PrimaDORAC: A free web interface for the assignment of partial charges, chemical topology, and bonded parameters in organic or drug molecules. *Journal of Chemical Information and Modeling* **2017**, *57*, 1240–1245.

(54) Jakalian, A.; Jack, D. B.; Bayly, C. I. Fast, efficient generation of high-quality atomic charges. AM1-BCC model: II. Parameterization and validation. *Journal of Computational Chemistry* **2002**, *23*, 1623–1641.

(55) Martínez, L.; Andrade, R.; Birgin, E.; Martínez, J. PACKMOL: A package for building

initial configurations for molecular dynamics simulations. *Journal of Computational Chemistry* **2009**, *30*, 2157–2164.

(56) Hockney, R. W.; Goel, S. P.; Eastwood, J. Quiet high resolution computer models of a plasma. *Journal of Computational Physics* **1974**, 148–158.

(57) Hess, B.; Kutzner, C.; Spoel, D.; Lindhal, E. GROMACS 4: Algorithms for highly efficient, load balanced, and scalable molecular dynamics simulation. *Journal of Chemical Theory and Computation* **2008**, *4*, 435–447.

(58) Darden, T.; York, D.; Pedersen, L. An N·log(N) method for Ewald sums in large systems. *Journal of Chemical Physics* **1993**, 10089–10092.

(59) Berendsen, H.; Postma, J.; van Gunsteren, W.; DiNola, A.; Haak, J. Molecular dynamics with coupling to an external bath. *Journal of Chemical Physics* **1984**, *81*, 3684.

(60) Hoover, W. Canonical dynamics: Equilibrium phase-space distributions. *Physical Review A* **1985**, *31*, 1695–1697.

(61) Walter, N. P.; Jaiswal, A.; Cai, Z.; Zhang, Y. LiquidLib: A comprehensive toolbox for analyzing classical and ab initio molecular dynamics simulations of liquids and liquid-like matter with applications to neutron scattering experiments. *Computer Physics Communications* **2018**, *228*, 209–218.

(62) Ozkanlar, A.; Clark, A. ChemNetworks: A complex network analysis tool for chemical systems. *Journal of Computational Chemistry* **2014**, *35*, 495–505.

(63) Dai, J.; Li, X.; Zhao, L.; Sun, H. Enthalpies of mixing predicted using molecular dynamics simulations and OPLS force field. *Fluid Phase Equilibria* **2010**, *289*, 156–165.

(64) Rafiee, H. R.; Frouzesh, F. The study of partial and excess molar volumes for binary mixtures of nitrobenzene and benzaldehyde with xylene isomers from T=(298.15 to 318.15) K and P= 0.087 MPa. *Journal of Advanced Research* **2016**, *7*, 769–780.

(65) Chandler, D. Interfaces and the driving force of hydrophobic assembly. *Nature* **2005**, *437*, 640–647.

(66) Widom, B.; Bhimalapuram, P.; Koga, K. The hydrophobic effect. *Physical Chemistry Chemical Physics* **2003**, *5*, 3085–3093.

(67) Lorenz, C. D.; Ziff, R. M. Precise determination of the bond percolation thresholds and finite-size scaling corrections for the sc, fcc, and bcc lattices. *Physical Review E* **1998**, *57*, 230–236.

(68) Servis, M. J.; Piechowicz, M.; Shkrob, I. A.; Soderholm, L.; Clark, A. E. Amphiphile Organization in Organic Solutions: An Alternative Explanation for Small-Angle X-ray Scattering Features in Malonamide/Alkane Mixtures. *The Journal of Physical Chemistry B* **2020**,

(69) Lenton, S.; Rhys, N. H.; Towey, J. J.; Soper, A. K.; Dougan, L. Temperature-dependent segregation in alcohol–water binary mixtures is driven by water clustering. *The Journal of Physical Chemistry B* **2018**, *122*, 7884–7894.

(70) Patel, N. C.; Sandler, S. I. Excess volumes of the water/methanol, n-heptane/ethyl acetate, n-heptane/n-butyraldehyde, and n-heptane/isobutyraldehyde systems. *Journal of Chemical and Engineering Data* **1985**, *30*, 218–222.

(71) Tanaka, H.; Gubbins, K. E. Structure and thermodynamic properties of water–methanol mixtures: Role of the water–water interaction. *The Journal of Chemical Physics* **1992**, *97*, 2626–2634.

(72) Koh, C. A.; Tanaka, H.; Walsh, J. M.; Gubbins, K. E.; Zollweg, J. A. Thermodynamic and structural properties of methanol-water mixtures: experiment, theory, and molecular simulation. *Fluid Phase Equilibria* **1993**, *83*, 51–58.

(73) González-Salgado, D.; Nezbeda, I. Excess properties of aqueous mixtures of methanol: Simulation versus experiment. *Fluid phase equilibria* **2006**, *240*, 161–166.

(74) Wakisaka, A.; Matsuura, K. Microheterogeneity of ethanol–water binary mixtures observed at the cluster level. *Journal of Molecular Liquids* **2006**, *129*, 25–32.

(75) Soper, A. K.; Dougan, L.; Crain, J.; Finney, J. L. Excess entropy in alcohol- water solutions: A simple clustering explanation. *The Journal of Physical Chemistry B* **2006**, *110*, 3472–3476.

(76) Tanaka, F.; Koga, T.; Winnik, F. M. Temperature-responsive polymers in mixed solvents: competitive hydrogen bonds cause cononsolvency. *Physical Review Letters* **2008**, *101*, 028302.

(77) Mochizuki, K.; Pattenaude, S. R.; Ben-Amotz, D. Influence of cononsolvency on the aggregation of tertiary butyl alcohol in methanol–water mixtures. *Journal of the American Chemical Society* **2016**, *138*, 9045–9048.

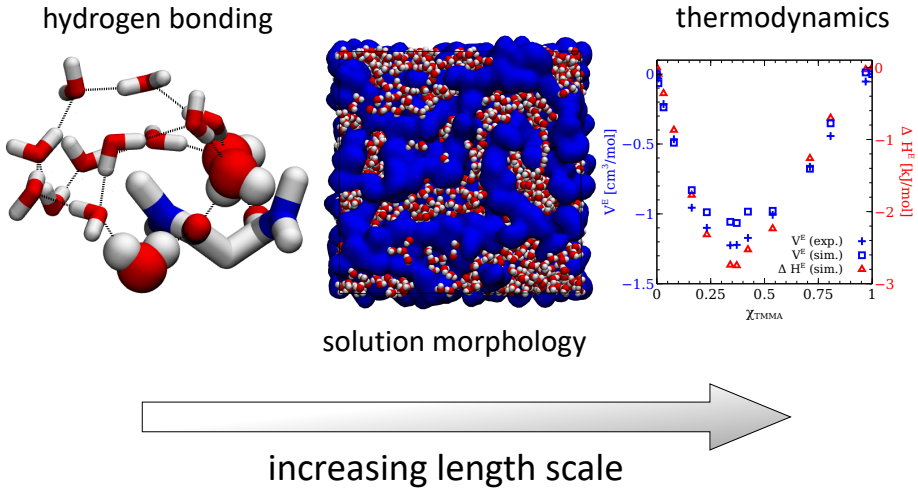
hydrogen bonding
thermodynamics
solution morphology
V^E [cm^3/mol]
Δ H^E [kJ/mol]
V^E (exp.)
V^E (sim.)
Δ H^E (sim.)
χ_TMMA
increasing length scale

TOC image.